Progress In Electromagnetics Research, PIER 23, 239–263, 1999

ELECTROMAGNETIC SCATTERING BY AN INHOMOGENEOUS CHIRAL SPHERE OF VARYING PERMITTIVITY: A DISCRETE ANALYSIS USING MULTILAYERED MODEL

L. W. Li, Y. Dan, and M. S. Leong

Communications and Microwave Division
Department of Electrical Engineering
National University of Singapore
10 Kent Ridge Crescent, Singapore 119260

J. A. Kong

Research Laboratory of Electronics and
Department of Electrical Engineering
Massachusetts Institute of Technology
Cambridge, MA 02139, USA

1. INTRODUCTION

Chiral media, which were discovered in the last century, have been of much scientific interest and many practical applications to scientists and engineers in many different fields (e.g., physics, chemistry, and

biology). The conventional and simple constitutive relations governing the electromagnetic fields in optically active chiral media no longer hold. Instead, more complex relationships between the electric- and the magnetic-field quantities will have to be used to analyze the behaviors of the macroscopic electromagnetic fields in the presence of chiral objects. Resulted in from numerous applications in the fields of electromagnetic scattering, antenna radiation, and radio propagation, much attention has been paid during the past a few decades to the interaction of electromagnetic fields with such chiral media. There has been a lot of research work contributing significantly to this field, for instance, those work associated with chiral media [1–6].

Among the research work associated with electromagnetic wave scattering by chiral objects, analytic solutions for electromagnetic scattering by chiral spheres [7–9], circular cylinder(s) [10–13], spherical shells [14, 15], and spheroid [16] are available in the literature. There has, to the best of our knowledge, been no analytic solution to an inhomogeneous or multilayered chiral sphere. This work is to obtain an analytic solution to the problem of the electromagnetic scattering by an inhomogeneous and/or multilayered chiral sphere.

In this paper, an analytic solution to the problem is obtained by applying the discrete analysis of multilayered structures to such an inhomogeneous chiral sphere. Fields in each region of the chiral sphere are obtained and expanded in terms of spherical vector wave functions. Their scattering coefficients are derived by applying boundary conditions at all the spherical interfaces and expressed in recursive coefficient matrices. To check the newly developed algorithm for verification of correctness, electromagnetic scattering by a chiral sphere is first calculated and its results are compared for with those in [9]. After that, two cases are considered, i.e., one is a two-layered sphere coated with a lossless chiral outer layer of parameters in [11], and the other is a two-layered sphere coated with a lossy outer chiral layer of parameters in [13]. Comparison are also made to show how the current technique works and what the accuracy is. After the algorithm developed in the current work is examined, an inhomogeneous chiral sphere whose permittivity varies against its radial distance is then considered. The chiral sphere is then discretized into ten layers, each of which is assumed to have approximately constant permittivity. The technique developed in the paper for a multilayered chiral sphere is then applied in the analysis. Although only four cases are considered herein, the

algorithm developed is actually applicable to a chiral sphere of other dimensions and material characteristics for both horizontal and vertical polarizations of the incident waves.

The paper is organized in the order given subsequently. In Section 2, the coupled wavefield equations in a chiral medium are decoupled. The electric and magnetic fields are then expanded in terms of spherical vector wave functions. The coefficients of scattered electromagnetic fields are derived in Section 3. The calculation of the normalized radar cross sections (RCS's) is carried out in Section 4. Numerical results are obtained in Section 5 for demonstrating the usefulness, effectiveness, and applicability of the method.

2. FORMULATION OF THE PROBLEM

2.1 The Wavefield Equations in Chiral Media

Consider a radially N-layered geometry of the chiral medium. The incident wave is assumed to be in the first region of the spherically N-layered medium. Without loss of generality, each region of the layered structure is assumed to be a chiral medium which is usually characterized by the following set of constitutive relations:

$$\boldsymbol{D}_f = \varepsilon_f \boldsymbol{E} - i\xi_f \boldsymbol{B}, \tag{1a}$$

$$\boldsymbol{H}_f = \frac{1}{\mu_f}\boldsymbol{B} - i\xi_f \boldsymbol{E}, \tag{1b}$$

where ε_f, μ_f, and ξ_f are the medium's permittivity, permeability and chirality parameters, respectively, and $f = 1, 2, \cdots, N$. The parameters, ε_f, μ_f and ξ_f, could be lossy (complex quantities) or lossless (real quantities). If $\xi_c = 0$, then (1a) and (1b) reduce to the constitutive relations for an achiral medium. To simplify the following developments, (1a) and (1b) are rewritten into

$$\boldsymbol{D}_f = \varepsilon_{fc} \boldsymbol{E} - i\mu_f \xi_f \boldsymbol{H}, \tag{2a}$$

$$\boldsymbol{B}_f = \mu_f \boldsymbol{H} + i\mu_f \xi_f \boldsymbol{E}, \tag{2b}$$

where the effective permittivity ϵ_{fc} is defined as

$$\epsilon_{fc} = \epsilon_f + \mu_f \xi_f^2. \tag{3}$$

In a chiral medium without source distributions, the wave equations after the aforementioned constitutive relations are substituted are

$$\nabla^2 \begin{bmatrix} \boldsymbol{E}_f \\ \boldsymbol{H}_f \end{bmatrix} + [k]^2 \begin{bmatrix} \boldsymbol{E}_f \\ \boldsymbol{H}_f \end{bmatrix} = 0, \tag{4a}$$

$$[k] = \begin{bmatrix} \omega\mu_f\xi_f & -j\omega\mu_f \\ j\omega\epsilon_{fc} & \omega\mu_f\xi_f \end{bmatrix}. \tag{4b}$$

By following Bohren's procedure [7], the coupling caused by $[k]$ in the wave equations can be removed by diagonalizing $[k]$ such that

$$[A]^{-1}[k][A] = \begin{bmatrix} k_f^{(R)} & 0 \\ 0 & -k_f^{(L)} \end{bmatrix}. \tag{5}$$

A simple form of [A] is then found to be

$$[A] = \begin{bmatrix} 1 & 1 \\ \dfrac{j}{\eta_f} & -\dfrac{j}{\eta_f} \end{bmatrix} \tag{6}$$

where the chiral wave impedance is given by:

$$\eta_f = \sqrt{\frac{\mu_f}{\epsilon_{fc}}} \tag{7}$$

and the propagation constant k_f in each layer of the multilayered medium is designated generally as

$$k_f^2 = \omega^2 \left(\mu_f\varepsilon_{fc} - \mu_f^2\xi_f\right). \tag{8a}$$

Hence, two circularly polarized modes present in the unbounded medium, i.e., the *r*ight- and *l*eft-handed *c*ircularly *p*olarized (RCP and LCP) waves, are obtained. Their corresponding wave numbers are given, respectively, by

$$k_f^{(R)} = \omega\mu_f\xi_f + \omega\sqrt{\mu_f\varepsilon_{fc}}, \tag{8b}$$

$$k_f^{(L)} = -\omega\mu_f\xi_f + \omega\sqrt{\mu_f\varepsilon_{fc}}. \tag{8c}$$

Now, let us define $(\boldsymbol{E}_R, \boldsymbol{E}_L)$ as

$$\begin{bmatrix} \boldsymbol{E}_f \\ \boldsymbol{H}_f \end{bmatrix} = [A] \begin{bmatrix} \boldsymbol{E}_f^{(R)} \\ \boldsymbol{E}_f^{(L)} \end{bmatrix}. \tag{9}$$

It has been shown that $\boldsymbol{E}_f^{(R)}$ and $\boldsymbol{E}_f^{(L)}$ are the electric fields of right and left circularly polarized waves with propagation constants $k_f^{(R)}$ and $k_f^{(L)}$. Thus, the decoupled source-free wave equation in chiral media is:

$$\nabla^2 \begin{bmatrix} \boldsymbol{E}_f^{(R)} \\ \boldsymbol{E}_f^{(L)} \end{bmatrix} + \begin{bmatrix} {k_R}^2 \boldsymbol{E}_f^{(R)} \\ {k_L}^2 \boldsymbol{E}_f^{(L)} \end{bmatrix} = 0. \tag{10}$$

2.2 The Eigenfunction Expansion

Consider a pair of incident electromagnetic waves of parallel (I) and perpendicular (II) polarizations. The incident waves propagate at an arbitrary angle α onto the chiral sphere whose center O is at the origin of Cartesian or spherical coordinates system. They are expressed by:

$$\boldsymbol{E}_I^i = E_I(\cos\alpha\widehat{\boldsymbol{x}} - \sin\alpha\widehat{\boldsymbol{z}})e^{ik_0(x\sin\alpha + z\cos\alpha)}, \tag{11a}$$

$$\boldsymbol{H}_I^i = \frac{k_0 E_I}{\omega\mu_0}\widehat{\boldsymbol{y}}e^{ik_0(x\sin\alpha + z\cos\alpha)}, \tag{11b}$$

and

$$\boldsymbol{E}_{II}^i = E_{II}\widehat{\boldsymbol{y}}e^{ik_0(x\sin\alpha + z\cos\alpha)}, \tag{12a}$$

$$\boldsymbol{H}_{II}^i = -\frac{k_0 E_{II}}{\omega\mu_0}(\cos\alpha\widehat{\boldsymbol{x}} - \sin\alpha\widehat{\boldsymbol{z}})e^{ik_0(x\sin\alpha + z\cos\alpha)}, \tag{12b}$$

where E_I and E_{II} are the amplitude of the incident electric fields of the parallel (I) and perpendicular (II) polarizations, α is the incident angle. It is assumed for convenience that the incident wave lies on the $\widehat{\boldsymbol{x}}\widehat{\boldsymbol{z}}$-plane, i.e., $\phi' = 0$. For easily match boundary conditions satisfied by the tangential field components on the spherical surfaces, the incident electromagnetic fields can be expanded in terms of spherical vector wave functions that are defined in the spherical coordinates system as follows:

$$\begin{aligned} \boldsymbol{M}_{\substack{e\\o}mn}(k) = &\mp \frac{mz_n(kr)}{\sin\theta}P_n^m(\cos\theta)\begin{matrix}\sin\\\cos\end{matrix} m\phi\widehat{\boldsymbol{\theta}} \\ &- z_n(kr)\frac{\partial P_n^m(\cos\theta)}{\partial\theta}\begin{matrix}\cos\\\sin\end{matrix} m\phi\widehat{\boldsymbol{\phi}}, \end{aligned} \tag{13a}$$

$$\begin{aligned}\boldsymbol{N}_{\substack{e\\o}mn}(k) =& \frac{n(n+1)z_n(kr)}{kr} P_n^m(\cos\theta) \begin{matrix}\cos\\ \sin\end{matrix} m\phi \widehat{\boldsymbol{r}} \\ &+ \frac{\partial[rz_n(kr)]}{kr\partial r} \frac{\partial P_n^m(\cos\theta)}{\partial\theta} \begin{matrix}\cos\\ \sin\end{matrix} m\phi \widehat{\boldsymbol{\theta}} \\ &\mp \frac{m}{\sin\theta} \frac{\partial[rz_n(kr)]}{kr\partial r} P_n^m(\cos\theta) \begin{matrix}\sin\\ \cos\end{matrix} m\phi \widehat{\boldsymbol{\phi}}, \end{aligned} \tag{13b}$$

where $z_n(kr)$ represents the spherical Bessel functions of n-order, and $P_n^m(\cos\theta)$ identifies the associated Legendre function of the first kind with the order (n, m).

The incident waves under the two polarizations have, as introduced by Morrison and Cross [17, 18], the following forms are derived:

$$\boldsymbol{E}_{\substack{I\\II}}^i = \sum_{n=1}^{\infty}\sum_{m=0}^{n} \left[P_{\substack{o\\e}mn}^i \boldsymbol{M}_{\substack{o\\e}mn}(k_0) + Q_{\substack{e\\o}mn}^i \boldsymbol{N}_{\substack{e\\o}mn}(k_0) \right], \tag{14a}$$

$$\boldsymbol{H}_{\substack{I\\II}}^i = \frac{ik_0}{\omega\mu_0} \sum_{n=1}^{\infty}\sum_{m=0}^{n} \left[P_{\substack{o\\e}mn}^i \boldsymbol{N}_{\substack{e\\o}mn}(k_0) + Q_{\substack{e\\o}mn}^i \boldsymbol{M}_{\substack{e\\o}mn}(k_0) \right], \tag{14b}$$

where the spherical Bessel functions of the first kind, i.e., $z_n(k_0 r) = j_n(k_0 r)$, are used in the above vector wave functions, the orthogonal properties of $\boldsymbol{M}_{\substack{e\\o}mn}(k_0)$ and $\boldsymbol{N}_{\substack{e\\o}mn}(k_0)$ are considered, and the coefficients of the expanded incident electromagnetic fields, $P_{\substack{e\\o}mn}^i$ and $Q_{\substack{e\\o}mn}^i$, are given by

$$P_{\substack{o\\e}mn}^i = (2-\delta_{m0})(-i)^n \mathcal{N}_{mn} \begin{Bmatrix} \dfrac{mP_n^m(\cos\alpha)}{\sin\alpha} E_I \\ -\dfrac{\partial P_n^m(\cos\alpha)}{\partial\alpha} E_{II} \end{Bmatrix}, \tag{15a}$$

$$Q_{\substack{e\\o}mn}^i = -(2-\delta_{m0})(-i)^{n+1} \mathcal{N}_{mn} \begin{Bmatrix} \dfrac{\partial P_n^m(\cos\alpha)}{\partial\alpha} E_I \\ \dfrac{mP_n^m(\cos\alpha)}{\sin\alpha} E_{II} \end{Bmatrix}, \tag{15b}$$

where δ_{mn} ($= 1$ for $m = n$; and 0 for $m \neq n$) denotes the Kronecker symbol, and $\mathcal{N}_{mn}$ is the normalization coefficient from the Legendre polynomial orthogonality relations given by

$$\mathcal{N}_{mn} = \frac{(2n+1)}{n(n+1)} \frac{(n-m)!}{(n+m)!}. \tag{16}$$

When $\alpha = 0^\circ$ or 180°, all the coefficients with $m \neq 1$ vanish, thus (15a) and (15b) reduce to

$$P^{i}_{\substack{o\\e}mn} = (-i)^n \begin{Bmatrix} \dfrac{2n+1}{n(n+1)} E_I \\ -\dfrac{2n+1}{n(n+1)} E_{II} \end{Bmatrix}, \tag{17a}$$

$$Q^{i}_{\substack{e\\o}mn} = -(-i)^{n+1} \begin{Bmatrix} \dfrac{2n+1}{n(n+1)} E_I \\ \dfrac{2n+1}{n(n+1)} E_{II} \end{Bmatrix}. \tag{17b}$$

The parallelly polarized waves in chiral media can be written in the form of eigenfunction expansion and considered as a superposition of right and left circularly polarized fields. The left- and right-handed circularly polarized fields can be expressed using spherical vector wave functions as:

$$\boldsymbol{E}^{(p)}_R = \boldsymbol{M}^{(p)}_{\substack{o\\e}mn}(k^{(R)}) + \boldsymbol{N}^{(p)}_{\substack{e\\o}mn}(k^{(R)}), \tag{18a}$$

$$\boldsymbol{E}^{(p)}_L = \boldsymbol{M}^{(p)}_{\substack{o\\e}mn}(k^{(L)}) - \boldsymbol{N}^{(p)}_{\substack{e\\o}mn}(k^{(L)}), \tag{18b}$$

where p equals 1 or 4. The superscript (1) represents the first type of spherical Bessel function and (4) denotes the second kind of spherical Hankel function. It is to be noted that the notations $\begin{smallmatrix} e\\o \end{smallmatrix}mn$ and $\begin{smallmatrix} o\\e \end{smallmatrix}mn$ of the dyadic in (18) have a different meaning from those in (14) where the upper (or lower) notation denotes the I parallel (or the II perpendicular) polarization. Hence in (18), it means the summation form of both even and odd modes should be taken into account.

The electric field and magnetic field in f-th region can be expressed in the following form:

$$\boldsymbol{E}^{(p)}_f = \boldsymbol{E}^{(p)}_{f,R} + \boldsymbol{E}^{(p)}_{f,L}, \tag{19a}$$

$$\boldsymbol{H}^{(p)}_f = j\eta_f^{-1}\boldsymbol{E}^{(p)}_{f,R} - j\eta_f^{-1}\boldsymbol{E}^{(p)}_{f,L}. \tag{19b}$$

Under the spherical coordinates, the electromagnetic fields usually consist of the radially outgoing- and incoming-propagation wave modes. Hence, the electric and magnetic fields in regions from the second layer

to the ($n-1$-th layer are expressed as:

$$\begin{aligned}\boldsymbol{E}_f =& C_{1f}\left[\boldsymbol{M}^{(4)}_{\substack{o\\e}mn}(k_f^{(R)}) + \boldsymbol{N}^{(4)}_{\substack{e\\o}mn}(k_f^{(R)})\right]\\ &+ C_{2f}\left[\boldsymbol{M}^{(4)}_{\substack{o\\e}mn}(k_f^{(L)}) - \boldsymbol{N}^{(4)}_{\substack{e\\o}mn}(k_f^{(L)})\right]\\ &+ C_{3f}\left[\boldsymbol{M}^{(1)}_{\substack{o\\e}mn}(k_f^{(R)}) + \boldsymbol{N}^{(1)}_{\substack{e\\o}mn}(k_f^{(R)})\right]\\ &+ C_{4f}\left[\boldsymbol{M}^{(1)}_{\substack{o\\e}mn}(k_f^{(L)}) - \boldsymbol{N}^{(1)}_{\substack{e\\o}mn}(k_f^{(L)})\right], \end{aligned} \tag{20a}$$

$$\begin{aligned}\boldsymbol{H}_f =& j\eta_f^{-1}\left[\boldsymbol{E}_{f,R} + \boldsymbol{E}_{f,L}\right]\\ =& j\eta_f^{-1}C_{1f}\left[\boldsymbol{M}^{(4)}_{\substack{o\\e}mn}(k_f^{(R)}) + \boldsymbol{N}^{(4)}_{\substack{e\\o}mn}(k_f^{(R)})\right]\\ &- j\eta_f^{-1}C_{2f}\left[\boldsymbol{M}^{(4)}_{\substack{o\\e}mn}(k_f^{(L)}) - \boldsymbol{N}^{(4)}_{\substack{e\\o}mn}(k_f^{(L)})\right]\\ &+ j\eta_f^{-1}C_{3f}\left[\boldsymbol{M}^{(1)}_{\substack{o\\e}mn}(k_f^{(R)}) + \boldsymbol{N}^{(1)}_{\substack{e\\o}mn}(k_f^{(R)})\right]\\ &- j\eta_f^{-1}C_{4f}\left[\boldsymbol{M}^{(1)}_{\substack{o\\e}mn}(k_f^{(L)}) - \boldsymbol{N}^{(1)}_{\substack{e\\o}mn}(k_f^{(L)})\right]. \end{aligned} \tag{20b}$$

While only the inward waves exist in the inner-most layer and the outward waves in the outer-most layer. Therefore, the coefficients corresponding to the outgoing waves in the inner-most layer and to the incoming waves in the outer-most layer must vanish. The electric field in the out-most and inner-most layer are written as follows, respectively:

$$\begin{aligned}\boldsymbol{E}_1 =& \boldsymbol{E}^i + \boldsymbol{E}^s\\ =& \boldsymbol{E}^i + C_{11}\left[\boldsymbol{M}^{(4)}_{\substack{o\\e}mn}(k_0) + \boldsymbol{N}^{(4)}_{\substack{e\\o}mn}(k_0)\right]\\ &+ C_{21}\left[\boldsymbol{M}^{(4)}_{\substack{o\\e}mn}(k_0) - \boldsymbol{N}^{(4)}_{\substack{e\\o}mn}(k_0)\right], \end{aligned} \tag{21a}$$

$$\begin{aligned}\boldsymbol{E}_n =& C_{3n}\left[\boldsymbol{M}^{(1)}_{\substack{o\\e}mn}(k_n^{(R)}) + \boldsymbol{N}^{(1)}_{\substack{e\\o}mn}(k_n^{(R)})\right]\\ &- C_{4n}\left[\boldsymbol{M}^{(1)}_{\substack{o\\e}mn}(k_n^{(L)}) - \boldsymbol{N}^{(1)}_{\substack{e\\o}mn}(k_n^{(L)})\right], \end{aligned} \tag{21b}$$

where k_0 stands for the free-space wave number outside the multilayered chiral sphere, given by

$$k_0 = \omega\sqrt{\mu_0\epsilon_0}. \tag{22}$$

3. DETERMINATION OF THE SCATTERING COEFFICIENTS

The electric and magnetic fields satisfy the following boundary conditions at the spherical interfaces $r = a_j$ ($j = 1, 2, \cdots, N-1$):

$$\widehat{\boldsymbol{r}} \times \boldsymbol{E}_f = \widehat{\boldsymbol{r}} \times \boldsymbol{E}_{(f+1)}, \tag{23a}$$

$$\widehat{\boldsymbol{r}} \times \boldsymbol{H}_f = \widehat{\boldsymbol{r}} \times \boldsymbol{H}_{(f+1)}. \tag{23b}$$

Without any loss of generality for the problem, we extend (23a)–(23b) into a linear equation system. To simplify the complicated algebraic calculations, let us introduce the following operators [6]

$$\Im_{im}^{(r,l)} = j_n(k_i^{(r,l)} a_m), \tag{24a}$$

$$\hbar_{im}^{(r,1)} = h_n^{(2)}(k_i^{(r,l)} a_m), \tag{24b}$$

$$\partial\Im_{im}^{(r,l)} = \frac{1}{\rho}\frac{d[\rho j_n(\rho)]}{d\rho}\bigg|_{\rho=k_i^{(r,l)}a_m}, \tag{24c}$$

$$\partial\hbar_{im}^{(r,1)} = \frac{1}{\rho}\frac{d[\rho h_n^{(2)}(\rho)]}{d\rho}\bigg|_{\rho=k_i^{(r,l)}a_m}; \tag{24d}$$

$$i = 1, 2, \cdots, N, \qquad m = 1, 2, \cdots, N-1.$$

Replacing the linear equation system by the coefficient transmission matrices, we have the following matrix equations

$$\mathbf{F}_f C_f = \mathbf{F}_{f+1} C_{f+1}, \tag{25}$$

where the parameter and coefficient matrices are defined as [6]:

$$\mathbf{F}_f = \begin{bmatrix} \partial\hbar_{ff}^{(r)} & -\partial\hbar_{ff}^{(l)} & \partial\Im_{ff}^{(r)} & -\partial\Im_{ff}^{(l)} \\ \hbar_{ff}^{(r)} & \hbar_{ff}^{(l)} & \Im_{ff}^{(r)} & \Im_{ff}^{(l)} \\ \eta_{fc}^{-1}\partial\hbar_{ff}^{(r)} & \eta_{fc}^{-1}\partial\hbar_{ff}^{(l)} & \eta_{fc}^{-1}\partial\Im_{ff}^{(r)} & \eta_{fc}^{-1}\partial\Im_{ff}^{(l)} \\ \eta_{fc}^{-1}\hbar_{ff}^{(r)} & -\eta_{fc}^{-1}\hbar_{ff}^{(l)} & \eta_{fc}^{-1}\Im_{ff}^{(r)} & -\eta_{fc}^{-1}\Im_{ff}^{(l)} \end{bmatrix}, \tag{26a}$$

$$\mathbf{C}_f = \begin{bmatrix} C_{1f} \\ C_{2f} \\ C_{3f} \\ C_{4f} \end{bmatrix}, \tag{26b}$$

$$\mathbf{F}_{f+1} = \begin{bmatrix} \partial\hbar^{(r)}_{(f+1)f} & -\partial\hbar^{(l)}_{(f+1)f} \\ \hbar^{(r)}_{(f+1)f} & \hbar^{(l)}_{(f+1)f} \\ \eta^{-1}_{(f+1)c}\partial\hbar^{(r)}_{(f+1)f} & \eta^{-1}_{(f+1)c}\partial\hbar^{(l)}_{(f+1)f} \\ \eta^{-1}_{(f+1)c}\hbar^{(r)}_{(f+1)f} & -\eta^{-1}_{(f+1)c}\hbar^{(l)}_{(f+1)f} \end{bmatrix}$$
$$\begin{bmatrix} \partial\Im^{(r)}_{(f+1)f} & -\partial\Im^{(l)}_{(f+1)f} \\ \Im^{(r)}_{(f+1)f} & \Im^{(l)}_{(f+1)f} \\ \eta^{-1}_{(f+1)c}\partial\Im^{(r)}_{(f+1)f} & \eta^{-1}_{(f+1)c}\partial\Im^{(l)}_{(f+1)f} \\ \eta^{-1}_{(f+1)c}\Im^{(r)}_{(f+1)f} & -\eta^{-1}_{(f+1)c}\Im^{(l)}_{(f+1)f} \end{bmatrix}, \tag{26c}$$

$$\mathbf{C}_{f+1} = \begin{bmatrix} C_{1(f+1)} \\ C_{2(f+1)} \\ C_{3(f+1)} \\ C_{4(f+1)} \end{bmatrix}, \tag{26d}$$

with

$$\eta^{-1}_{fc} = \sqrt{\frac{\varepsilon_{fc}}{\mu_f}}, \tag{27a}$$

$$\eta^{-1}_{(f+1)c} = \sqrt{\frac{\varepsilon_{(f+1)c}}{\mu_{f+1}}}. \tag{27b}$$

To simplify the derivation of the coefficients , we found the inverse of $\mathbf{F}_{f+1}$ by using commercially available softwares with symbolic calculations such as *Mathematica*.

We can rewrite the linear matrix equation (26) into the following form [6]

$$C_{f+1} = \mathbf{T}_f C_f \tag{28}$$

where the transmission matrix in the eigen-expansion domain is given by:

$$\mathbf{T}_f = \mathbf{F}^{-1}_{f+1}\mathbf{F}_f = \left[T^f_{j\ell}\right]_{4\times4}. \tag{29}$$

For convenience and simplification, let us assume that

$$\mathbf{T}^{(k)} = \left[\mathcal{T}^{(k)}_{j\ell}\right]_{4\times4} = [\mathbf{T}_{N-1}][\mathbf{T}_{N-2}]\cdots[\mathbf{T}_{k+1}][\mathbf{T}_k]. \tag{30}$$

According to equation (29), we have the relation

$$\mathbf{C}_n = [\mathbf{T}_{N-1}\mathbf{T}_{N-2}\cdots\mathbf{T}_2\mathbf{T}_1]\,\mathbf{C}_1 \tag{31}$$

which can be rewritten as:

$$\mathbf{C}_n = \mathbf{T}^{(1)}\mathbf{C}_1 \tag{32}$$

where

$$\mathbf{C}_n = \begin{bmatrix} 0 \\ 0 \\ C_{3n} \\ C_{4n} \end{bmatrix}, \tag{33a}$$

$$\mathbf{T}^{(1)} = \begin{bmatrix} \mathcal{T}_{11}^{(1)} & \mathcal{T}_{12}^{(1)} & \mathcal{T}_{13}^{(1)} & \mathcal{T}_{14}^{(1)} \\ \mathcal{T}_{21}^{(1)} & \mathcal{T}_{22}^{(1)} & \mathcal{T}_{23}^{(1)} & \mathcal{T}_{24}^{(1)} \\ \mathcal{T}_{31}^{(1)} & \mathcal{T}_{32}^{(1)} & \mathcal{T}_{33}^{(1)} & \mathcal{T}_{34}^{(1)} \\ \mathcal{T}_{41}^{(1)} & \mathcal{T}_{42}^{(1)} & \mathcal{T}_{43}^{(1)} & \mathcal{T}_{44}^{(1)} \end{bmatrix}, \tag{33b}$$

$$\mathbf{C}_1 = \begin{bmatrix} C_{11} \\ C_{21} \\ C_{31} \\ C_{41} \end{bmatrix}. \tag{33c}$$

For simplicity, only the formulation for the parallelly polarized incident wave is shown and the electric-field intensity is assumed to be of unit amplitude. For the perpendicularly polarized incident wave, the same procedure follows. The incident wave of the parallel polarization has the following forms:

$$\boldsymbol{E}^i = \sum_{n=1}^{\infty}\sum_{m=0}^{n}\left[P_{omn}^i \boldsymbol{M}_{omn}^{(1)}(k_0) + Q_{emn}^i \boldsymbol{N}_{emn}^{(1)}(k_0)\right], \tag{34a}$$

$$\boldsymbol{H}^i = \frac{ik_0}{\omega\mu_0}\sum_{n=1}^{\infty}\sum_{m=0}^{n}\left[P_{omn}^i \boldsymbol{N}_{omn}^{(1)}(k_0) + Q_{emn}^i \boldsymbol{M}_{emn}^{(1)}(k_0)\right]. \tag{34b}$$

Based on the equations (14a) and (21a), we obtain :

$$C_{31} = \frac{P_{omn}^i + Q_{emn}^i}{2}, \tag{35a}$$

$$C_{41} = \frac{P_{omn}^i - Q_{emn}^i}{2}. \tag{35b}$$

From Eqs. (29) to (34), we can derive the scattering coefficients, C_{11} and C_{12}, as follows:

$$C_{11} = \left[P^i_{omn} + Q^i_{emn}\right] \frac{\mathcal{T}^{(1)}_{13}\mathcal{T}^{(1)}_{22} - \mathcal{T}^{(1)}_{23}\mathcal{T}^{(1)}_{12}}{2\left[\mathcal{T}^{(1)}_{12}\mathcal{T}^{(1)}_{21} - \mathcal{T}^{(1)}_{11}\mathcal{T}^{(1)}_{22}\right]} + \left[P^i_{omn} - Q^i_{emn}\right] \frac{\mathcal{T}^{(1)}_{14}\mathcal{T}^{(1)}_{22} - \mathcal{T}^{(1)}_{24}\mathcal{T}^{(1)}_{12}}{2\left[\mathcal{T}^{(1)}_{12}\mathcal{T}^{(1)}_{21} - \mathcal{T}^{(1)}_{11}\mathcal{T}^{(1)}_{22}\right]}, \tag{36a}$$

$$C_{21} = \left[P^i_{omn} + Q^i_{emn}\right] \frac{\mathcal{T}^{(1)}_{11}\mathcal{T}^{(1)}_{23} - \mathcal{T}^{(1)}_{13}\mathcal{T}^{(1)}_{21}}{2\left[\mathcal{T}^{(1)}_{12}\mathcal{T}^{(1)}_{21} - \mathcal{T}^{(1)}_{11}\mathcal{T}^{(1)}_{22}\right]} + \left[P^i_{omn} - Q^i_{emn}\right] \frac{\mathcal{T}^{(1)}_{11}\mathcal{T}^{(1)}_{24} - \mathcal{T}^{(1)}_{14}\mathcal{T}^{(1)}_{21}}{2\left[\mathcal{T}^{(1)}_{12}\mathcal{T}^{(1)}_{21} - \mathcal{T}^{(1)}_{11}\mathcal{T}^{(1)}_{22}\right]}. \tag{36b}$$

The scattered electric field can be then written as:

$$\boldsymbol{E}^s = C_m \boldsymbol{M}^{(4)}_{omn}(k_0) + C_n \boldsymbol{N}^{(4)}_{emn}(k_0) \tag{37}$$

where

$$C_m = C_{11} + C_{21}, \tag{38a}$$

$$C_n = C_{11} - C_{21}. \tag{38b}$$

4. RADAR CROSS SECTION

The bistatic cross section is defined as

$$\sigma(\theta, \phi) = \lim_{r\to\infty} \left[4\pi r^2 \frac{|E^s|^2}{|E^i|^2}\right], \tag{39}$$

in which $|E^s|$ and $\left|E^i\right|$ are the amplitudes of scattered and incident electric fields, respectively. The normalized bistatic cross section is so defined as

$$\sigma(\theta, \phi)_{\text{normal}} = \frac{\sigma}{\pi a^2}, \tag{40}$$

where a is the outmost radius of the multilayered chiral sphere.

By using the asymptotic form of Hankel function for large argument given as follows:

$$h_n^{(2)}(kr) = j^{n+1}\frac{e^{-jkr}}{kr}, \tag{41a}$$

$$\frac{d[(kr)h_n^{(2)}(kr)]}{(kr)(d(kr)} = j^n\frac{e^{-jkr}}{kr}, \tag{41b}$$

the normalized bistatic cross section can be expressed as:

$$\frac{\pi\sigma(\theta,\phi)}{\lambda^2} = |F_\theta(\theta,\phi)|^2 + |F_\phi(\theta,\phi)|^2, \tag{42}$$

where

$$F_\theta(\theta,\phi) = \sum_{n=1}^{\infty}\sum_{m=0}^{n} j^n\left[jC_m P_n^m(\cos\theta)\frac{m}{\sin\theta} + C_n\frac{\partial P_n^m(\cos\theta)}{\partial\theta}\right]\cos(m\phi), \tag{43a}$$

$$F_\phi(\theta,\phi) = -\sum_{n=1}^{\infty}\sum_{m=0}^{n} j^n\left[jC_m\frac{\partial P_n^m(\cos\theta)}{\partial\theta} + C_n P_n^m(\cos\theta)\frac{m}{\sin\theta}\right]\sin(m\phi). \tag{43b}$$

5. NUMERICAL RESULTS

To show how the approach can be implemented numerically, an algorithm in its syntax form has been developed under the environment of *Mathematica* package. Numerical results are illustrated in this section. It is found that generally, the normalized bistatic cross sections are dependent upon various parameters characterizing the geometry, the material properties, and the incident fields.

The normalized radar cross section versus θ for a single (or so-called one-layered) sphere is plotted in Fig. 1. The second curve represents our results whereas the first curve shows the results of Rojas [9] computed by the method of integral equation. The comparison shows clearly that results from our method are quite close to those by Rojas for θ ranging from 0° to 90°. For the other range from 90° to 180°, our full-wave results are more accurate than those from the approximate integral equation method. This check serves as a partial and first confirmation of our method, formulation, and algorithm.

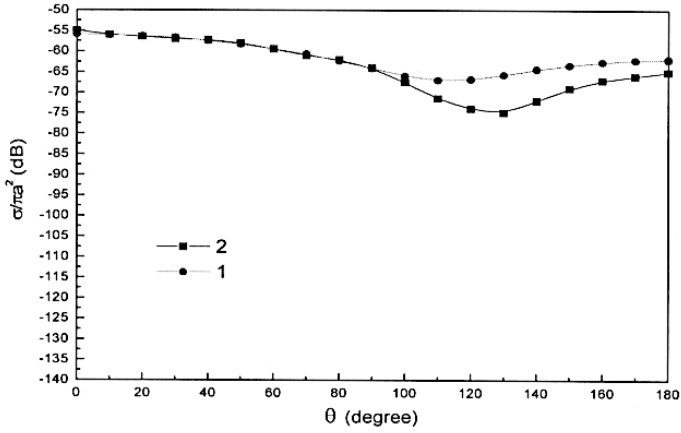

Figure 1. Comparison between the results for a chiral sphere by Rojas and those by our method. (1) our results and (2) results from Rojas using the integral equation method [9].

After we have verified the correctness of our method, formulation, and algorithm, subsequently, we will make four applications. In order for our results to be comparable, we have chosen some known sets of chiral parameters in our analysis.

In the first application, we consider a two-layered sphere coated with a lossless chiral outer layer. Fig. 2 shows the variation of the normalized bistatic cross section versus the spherical polar angle θ at different incident angles. The radii of the two-layered sphere are 25 cm and 75 cm respectively, and the operating frequency used is 300 MHz. The inner-most layer is isotropic with relative dielectric constant of $\epsilon_r = 2.0$ and relative permeability of $\mu_r = 1.0$. The out-layer is a chiral layer with $\epsilon_r = 3.0$ and $\mu_r = 2.0$ [11]. Fig. 3(a) presents the normalized RCS pattern in the $\phi = 0$-plane for $\xi = 0.001$ and Fig. 3(b) shows that in the $\phi = \frac{\pi}{2}$-plane for the same ξ. The RCS variation is also obtained and plotted for the cases of various plane wave incident angles at end-fire ($\alpha = 0^\circ$) and other α's of 30°, 60°, and 90° respectively. As the incident angle is equal to 90°, a symmetric variation has been exhibited.

In the second application, we also consider a two-layered sphere but coated with a lossy chiral outer layer. Fig. 3 depicts the variation of the normalized bistatic cross section with respect to θ at different incident angles. The radii of the two-layered sphere are $0.1\lambda_0$ and

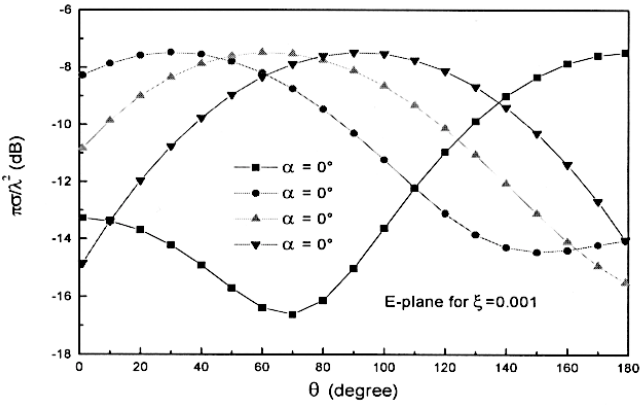

(a) E-plane

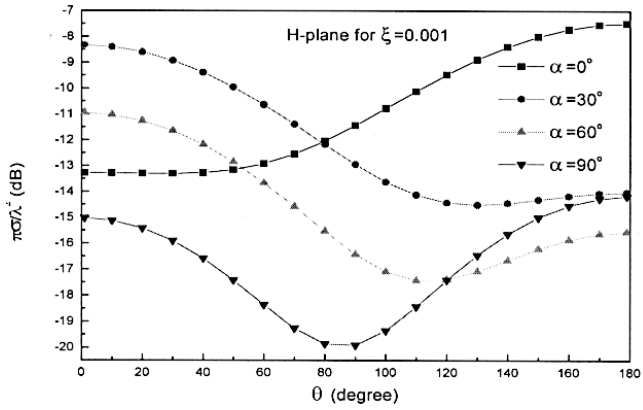

(b) H-plane

Figure 2. Normalized radar cross section versus θ for two-layered sphere with a lossless chiral outer layer for incident wave of parallel polarization. $\omega = 300\,\text{MHz}$, $a_1 = 0.75\,\text{m}$, $a_2 = 0.5\,\text{m}$, $\epsilon_2 = 3.0\epsilon_0$, $\mu_2 = 2.0\mu_0$, $\epsilon_3 = 2.0\epsilon_0$, $\mu_3 = \mu_0$, and $\xi = 0.001$. (a) $\phi = 0$-plane, and (b) $\phi = \frac{\pi}{2}$-plane.

$0.4\lambda_0$, respectively. The relative dielectric constant ϵ_r of the chiral material is chosen as $\epsilon_r = (3.0 - 0.15i)$, and the relative permeability is $\mu_r = (2.0 - 0.1i)$ [9]. The isotopic inner-most layer has a relative permittivity and a relative permeability of 2.0 and 1.0, respectively. Fig. 4(a) shows the RCS's in the $\phi = 0$-plane for $\xi = 0.001$ while Fig. 4(b) those in the $\phi = \frac{\pi}{2}$-plane for the same ξ. Four RCS values

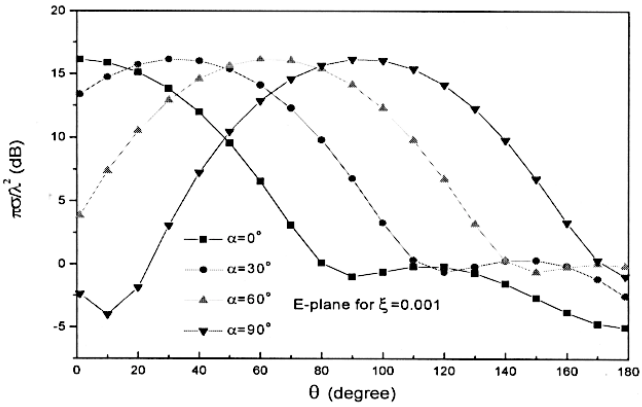

(a) E-plane

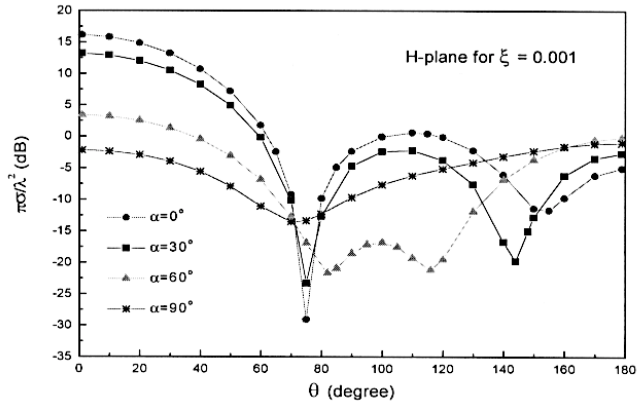

(b) H-plane

Figure 3. Normalized radar cross section versus spherical polar angle θ for a two-layered sphere with a lossy chiral outer layer for incident wave of parallel polarization. $a_1 = 0.4\lambda_0$, $a_2 = 0.1\lambda_0$, $\epsilon_2 = (3.0 - 0.15i)\epsilon_0$, $\mu_2 = (2.0 - 0.1i)\mu_0$, $\epsilon_3 = 2.0\epsilon_0$, $\mu_3 = \mu_0$, and $\xi = 0.001$. (a) $\phi = 0$-plane, and (b) $\phi = \frac{\pi}{2}$-plane.

at the same incident angle are computed. A valley is observed at the resonance around 75° in the $\phi = \frac{\pi}{2}$-plane at incident angles of both 0° and 30°. As α increases, the maximum of the scattering cross section moves toward $\theta = 180^\circ$ in the $\phi = 0$-plane.

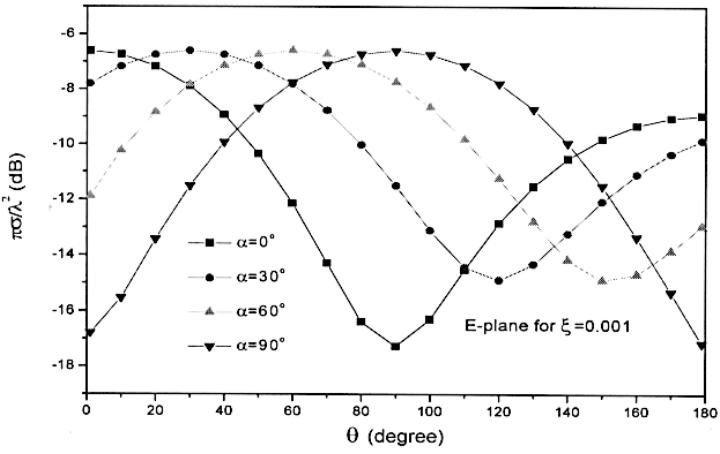

(a) E-plane

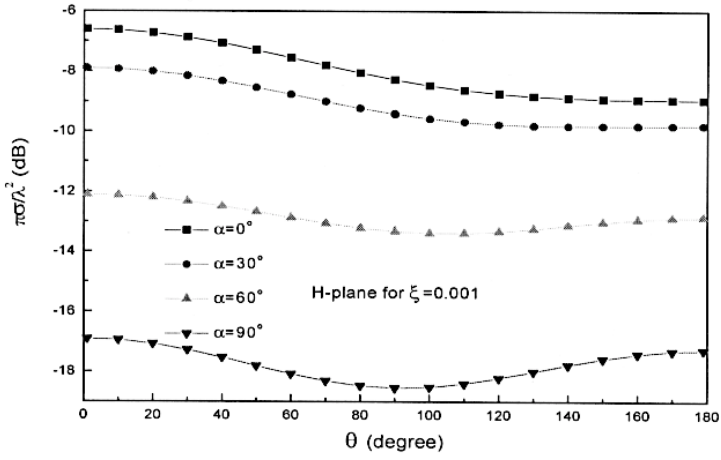

(b) H-plane

Figure 4. Normalized radar cross section versus θ for ten-layered sphere for incident wave of parallel polarization. $\omega = 3\,\mathrm{GHz}$, $a = 10\,\mathrm{cm}$, $\epsilon(r) = 2\epsilon_0(1 + 40r^2 + 100r^3)$ (r in meter), $\mu = \mu_0$, and $\xi = 0.001$. (a) $\phi = 0$-plane, and (b) $\phi = \frac{\pi}{2}$-plane.

In the third application, a radially inhomogeneous sphere is considered in which the relative permittivity varies with the radial distance inside the sphere. We divide the sphere into ten layers so that the permittivity in each layer can be proximately considered as a constant. The dielectric constant varies nonlinearly with the radial distance r, for instance, $\epsilon = 2\epsilon_0(1 + 40r^2 + 100r^3)$, the permeability is assumed as μ_0. Fig. 4(a) depicts the RCS's on different incident angle in the $\phi = 0$-plane for $\xi = 0.001$ while Fig. 4(b) those in the $\phi = \frac{\pi}{2}$-plane for the same ξ. Four incident angles are considered, too. As α increases, the maxima in the scattering patterns move toward $\theta = 180^o$ for scattering cross section in the $\phi = 0$-plane whereas the minima in the scattering patterns move toward $\theta = 0^\circ$ for scattering cross section in the $\phi = \frac{\pi}{2}$ plane.

To gain insight into the effects of varying the chiral admittances ξ_c, several values of chiral admittances are considered in the analysis, i.e., 0.0005, 0.001, 0.0015 and 0.002. For the purpose of comparison, the achiral case (where $\xi_c = 0$) has also been included. From Fig. 5 to Fig. 7, the normalized RCS versus chiral admittances for the aforementioned three cases are showed. Incident angle considered here is 60°. As the chiral admittance increases, an increase in magnitude of the scattering cross sections is observed in both the $\phi = 0$- and $\phi = \frac{\pi}{2}$-planes for the first and third cases. Whereas for the second case, the feature of RCS's becomes more complicated. In both $\phi = 0$- and $\phi = \frac{\pi}{2}$-planes, when ξ increases to 0.002, the maxima in magnitude of the RCS are no longer present. In $\phi = 0$-plane, the RCS values have the maxima between 0° and 110° when $\xi = 0.001$. The RCS values for $\xi = 0.002$ even have the minimum when θ is from 30° to the vicinity of 78°. This is contrary to the first and third case. For the first case, a deep is observed in $\phi = 0$ plane in the vicinity of 140°. And for the second case, a valley is found in the $\phi = \frac{\pi}{2}$-plane at about 155°. It can be seen that for these two cases, as chiral admittance increases the wave absorption characteristics is lessened. It is obvious that the chiral admittance affects the scattering and absorption characteristics. This is in good agreement with [8].

For a ten-layered chiral sphere, the incident wave of perpendicular polarization is included in our consideration. Fig. 8(a) illustrates the RCS in the $\phi = 0$ plane for $\xi = 0.001$ and 0.002. The RCS in the $\phi = \frac{\pi}{2}$ plane for $\xi = 0.001$ and 0.002 is shown in Fig. 8(b). The radius of the sphere is 10 cm and the incident angle is 90°. As the

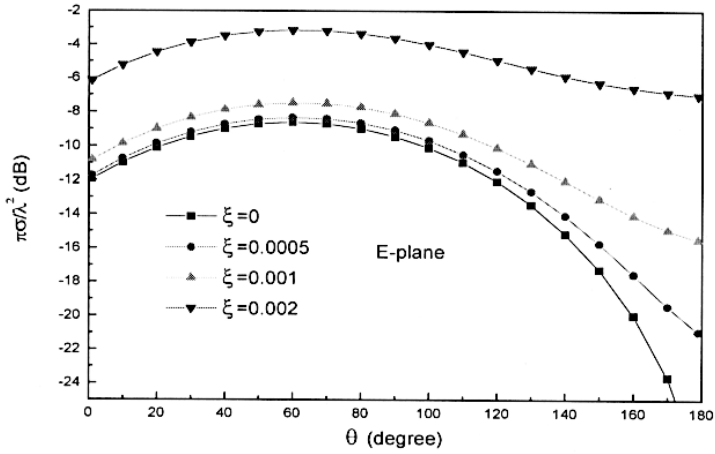

(a) E-plane

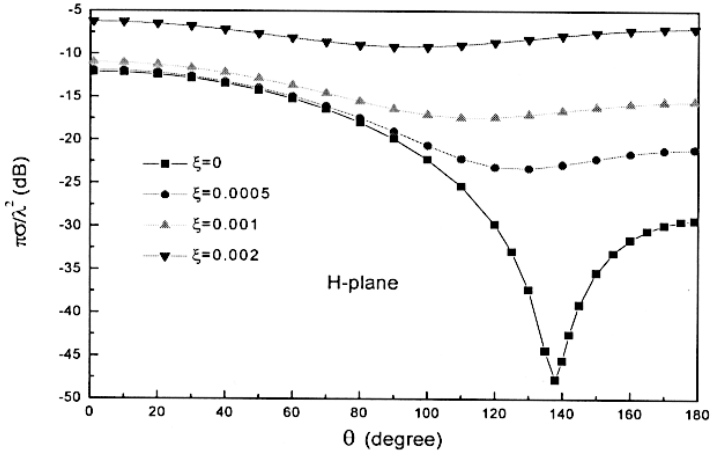

(b) H-plane

Figure 5. Normalized radar cross section versus θ and ξ for a two-layered sphere coated with a lossless chiral outer layer for incident wave of parallel polarization. $\omega = 300\,\mathrm{MHz}$, $a_1 = 0.75\,\mathrm{m}$, $a_2 = 0.5\,\mathrm{m}$, $\epsilon_2 = 3.0\epsilon_0$, $\mu_2 = 2.0\mu_0$, $\epsilon_3 = 2.0\epsilon_0$, $\mu_3 = \mu_0$, and incident angle $\alpha = 60^\circ$. (a) $\phi = 0$-plane, and (b) $\phi = \frac{\pi}{2}$-plane.

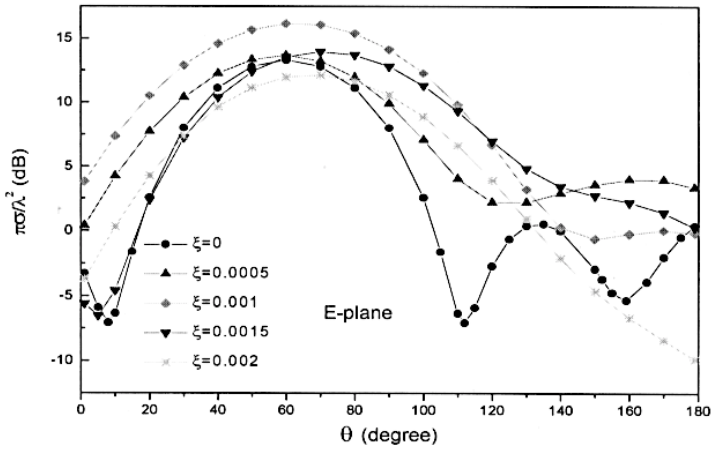

(a) E-plane

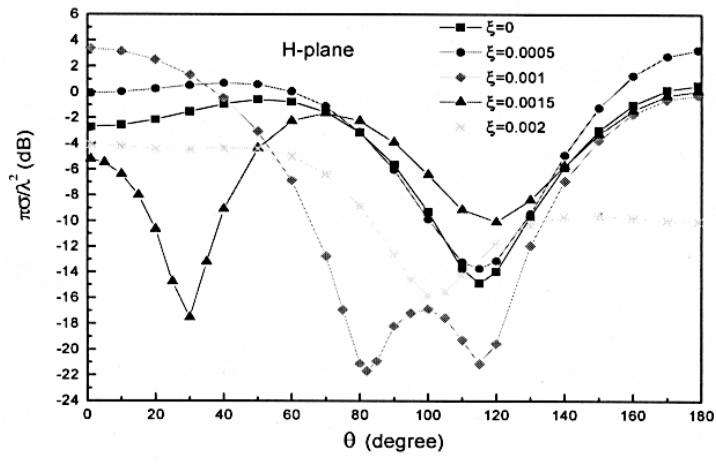

(b) H-plane

Figure 6. Normalized radar cross section versus θ and ξ for a two-layered sphere with a lossless chiral outer layer for incident wave of parallel polarization. $a_1 = 0.4\lambda_0$, $a_2 = 0.1\lambda_0$, $\epsilon_2 = (3.0 - 0.15i)\epsilon_0$, $\mu_2 = (2.0 - 0.1i)\mu_0$, $\epsilon_3 = 2.0\epsilon_0$, $\mu_3 = \mu_0$ and incident angle $\alpha = 60^\circ$. (a) $\phi = 0$-plane, and (b) $\phi = \frac{\pi}{2}$-plane.

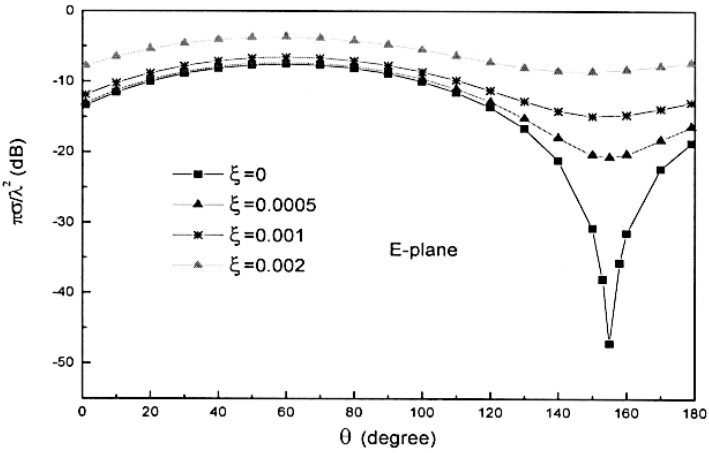

(a) E-plane

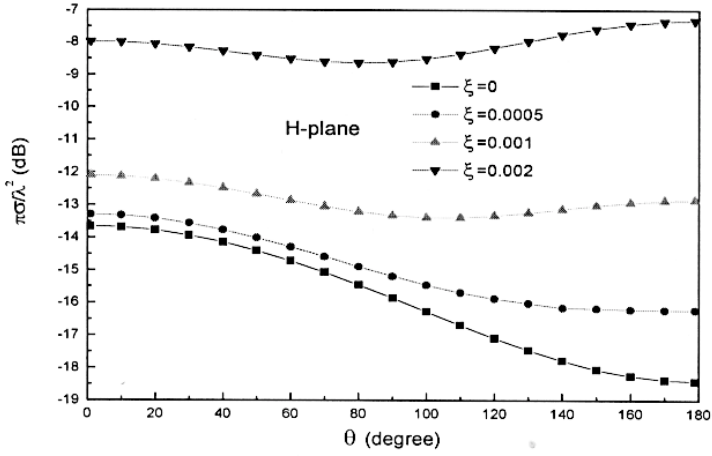

(b) H-plane

Figure 7. Normalized radar cross section (RCS) versus θ and ξ for ten-layered sphere for incident wave of perpendicular polarization. $\omega = 3\,\text{GHz}$, $a = 10\,\text{cm}$, $\epsilon(r) = 2\epsilon_0(1+40r^2+100r^3)$ (r in meter), $\mu = \mu_0$, and incident angle $\alpha = 60^\circ$. (a) $\phi = 0$-plane, and (b) $\phi = \frac{\pi}{2}$-plane.

chiral admittance increases, an increase in magnitude of the scattering cross sections is observed in both the $\phi = 0$- and $\phi = \frac{\pi}{2}$-planes for incident waves of two polarizations.

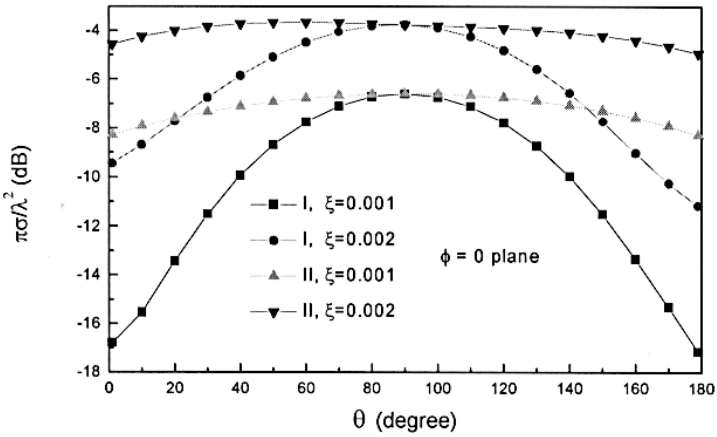

(a) E-plane

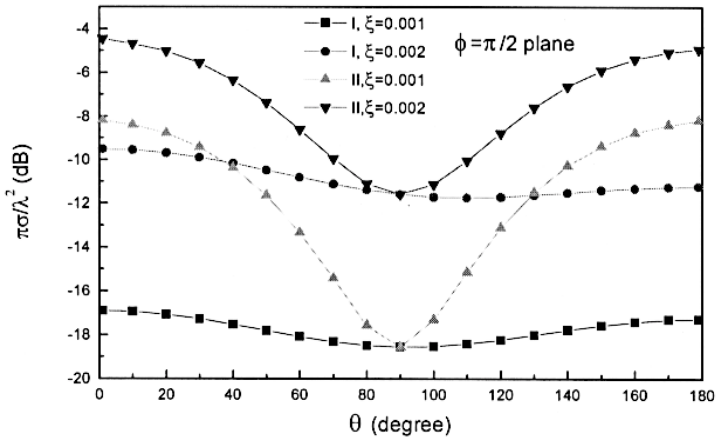

(b) H-plane

Figure 8. Normalized radar cross section versus θ for a ten-layered chiral sphere for incident waves of both parallel (I) and perpendicular (II) polarizations. $\omega = 3\,\mathrm{GHz}$, $a = 10\,\mathrm{cm}$, $\epsilon(r) = 2\epsilon_0(1+40r^2+100r^3)$ (r in meter), $\mu = \mu_0$, $\xi = 0.001$, and incident angle $\alpha = 90^\circ$. (a) $\phi = 0$-plane, and (b) $\phi = \frac{\pi}{2}$-plane.

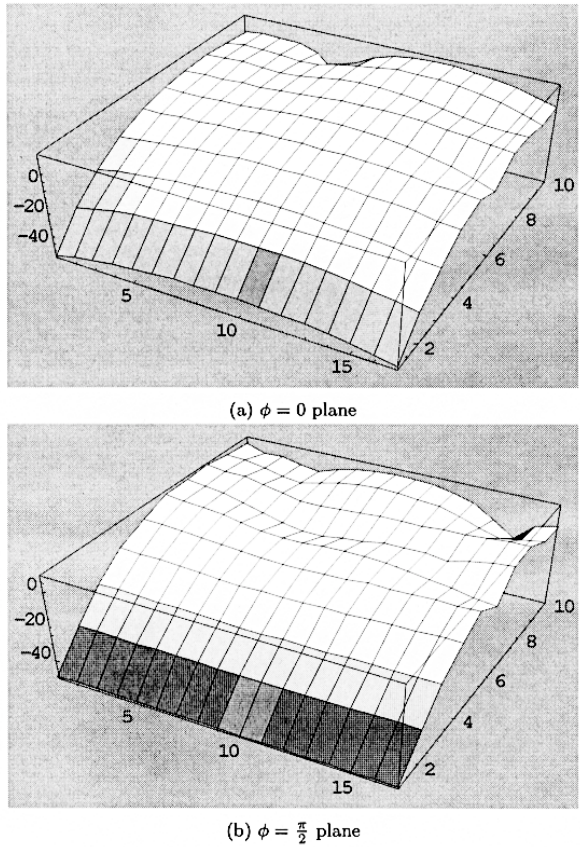

Figure 9. A 3-D plot of normalized radar cross section versus θ and frequency for a ten-layered sphere for incident wave of parallel polarization. $\omega = 3$ GHz, a=10 cm, $\epsilon(r) = 2\epsilon_0(1+40r^2+100r^3)$ (r in meter), $\mu = \mu_0$, $\xi = 0.001$, and incident angle $\alpha = 90^\circ$. (a) $\phi = 0$-plane, and (b) $\phi = \frac{\pi}{2}$-plane .

Fig. 9 shows a three dimensional plot of normalized RCS for a ten-layered sphere in the frequency band from 1 GHz to 10 GHz. Figs. 9(a) and 9(b) illustrate RCS in $\phi = 0$ plane and $\phi = \frac{\pi}{2}$, respectively. The chiral admittance is assumed to be 0.001 while the incident angle is 90^o . The normalized RCS changes in a larger range with respect to θ when the operating frequency increases.

Although four cases (one for algorithm verification and the other three for applications) are considered in the numerical analysis in the

paper, the formulation and the computer program are applicable to any other multilayered spherical geometries with different material parameters.

6. CONCLUSIONS

This paper has presented an efficient technique using the discretized multiple layer structure to obtain analytic solutions to the electromagnetic scattering by an inhomogeneous and/or multilayer chiral sphere for both incident waves of the parallel and perpendicular polarizations. The coupled wave equation for chiral media are transformed first into a set of decoupled wave equations so that classical eigenfunction techniques could be employed. The analysis is quite generalized for arbitrarily multilayered chiral spheres, applicable to a chiral sphere of any size and of any number of layers at any operating frequency. Each of the layer or region could be lossy or lossless, and it can also be inhomogeneous or homogeneous. The incident angle of two polarized waves is assumed to be arbitrary. Numerically, the solution requires the computation of M 4×4-matrices for an M-layer sphere. Numerical results illustrate that the chirality of the sphere plays a significant role on the scattered field. For a lossy chiral sphere, the RCS values change in a larger range than that for a lossless sphere. It is realized from the numerical computation that more summations are needed to achieve convergence if we consider a chiral sphere of larger size or at a higher frequency.

REFERENCES

1. Jaggard, J., A. R. Mickelson, and C. H. Papas, "On electromagnetic waves in chiral media," *Appl. Phys.*, Vol. 18, 211–216, 1978.
2. Vegni, L., R. Cicchetti, and P. Capece, "Spectral dyadic green's function formulation for planar integrated structures," *IEEE Trans. Antennas Propagat.*, Vol. AP-36, 1057–1065, 1988.
3. Engheta, N., and P. Pelet, "Modes in chirowaveguides," *Opt. lett.*, Vol. 14, 593–595, 1990.
4. Engheta, N., and M. W. Kowarz, "Antenna radiation in the presence of a chiral sphere," *J. Appl. Phys.*, Vol. 67, No. 2, 1057–1065, 1990.
5. Ren, W., "Dyadic green's functions and dipole radiations in layered chiral media," *J. Appl. Phys.*, Vol. 75, No. 1, 30–35, 1994.

6. Li, L. W., P. S. Kooi, M. S. Leong, and T. S. Yeo, "A general expression of dyadic green's functions in radially multilayered chiral media," *IEEE Trans. Antennas Propag.*, Vol. 43, No. 3, 232–238, 1995.
7. Bohren, C. F., "Light scattering by an optically active sphere," *Chem. Phys. Lett.*, Vol. 29, 458–462, 1974.
8. Lakhtakia, A., V. K. Varadan, and V. V. Varadan, "Scattering and absorption characteristics of lossy dielectric, chiral, nonspherical objects," *Appl. Opt.*, Vol. 24, 4146–4154, 1985.
9. Rojas, R. G., "Integral equations for the scattering by a three dimensional inhomogeneous chiral body," *J. Electromagn. Waves Applic.*, Vol. 6, No. 5/6, 733–750, 1992.
10. Bohren, C. F., "Scattering of electromagnetic waves by an optically active cylinder," *J. Colloid Interface Sci.*, Vol. 66, 101–109, 1974.
11. Kluskens, M. S., and E. H. Newman, "Scattering by a multilayer chiral cylinder," *IEEE Trans. Antennas Propag.*, Vol. 39, 91–96, 1991.
12. Graglia, R. D., P. L. E. Uslenghi, and C. L. Yu, "Electromagnetic oblique scattering by a cylinder coated with chiral layers and anisotropic jump-immittance sheets," *J. Electromagn. Waves Applic.*, Vol. 6, No. 5/6, 695–719, 1992.
13. Chen, Z., W. Hong, and W. Zhang, "Electromagnetic scattering from a chiral cylinder-general case," *IEEE Trans. Antennas Propag.*, Vol. 44, No. 7, 912–917, 1996.
14. Bohren, C. F., "Scattering of electromagnetic waves by an optically active spherical shell," *J. Chem. Phys.*, Vol. 62, 1566–1571, 1975.
15. Li, L. W., M. S. Leong, P. S. Kooi, T. S. Yeo, and Y. L. Qiu, "Radiation of an aperture antenna covered by a spherical shell chiral radome and fed by a circular waveguide," *IEEE Trans. on Antennas Propagat.*, Vol. 46, No. 5, 664–671, May 1998.
16. Cooray, M. F., and I. R. Ciric, "Wave scattering by a chiral spheroid," *J. Opt. Soc. Am. A*, Vol. 10, No. 6, 1197–1203, June 1993.
17. Morrison, J. A., and M. J. Cross, "Scattering of a plane electromagnetic wave by axisymmetric raindrops," *Bell Syst. Tech. J.*, Vol. 53, 955–1019, 1974.
18. Li, L. W., P. S. Kooi, M. S. Leong, T. S. Yeo, and M. Z. Gao, "Microwave attenuation by realistically distorted raindrops: Part I–Theory," *IEEE Trans. Antennas Propagat.*, Vol. 43, No. 8, 811–822, August 1995.